



Lesion location and lesion creation affect outcomes after focused ultrasound thalamotomy

✉ David J. Segar,¹ ✉ Asad M. Lak,¹ Shane Lee,² Maya Harary,³ Vamsidhar Chavakula,¹ ✉ Peter Lauro,² Nathan McDannold,⁴ Jason White⁴ and G. Rees Cosgrove¹

MRI-guided focused ultrasound thalamotomy has been shown to be an effective treatment for medication refractory essential tremor. Here, we report a clinical-radiological analysis of 123 cases of MRI-guided focused ultrasound thalamotomy, and explore the relationships between treatment parameters, lesion characteristics and outcomes. All patients undergoing focused ultrasound thalamotomy by a single surgeon were included. The procedure was performed as previously described, and patients were followed for up to 1 year. MRI was performed 24 h post-treatment, and lesion locations and volumes were calculated.

We retrospectively evaluated 118 essential tremor patients and five tremor-dominant Parkinson's disease patients who underwent thalamotomy. At 24 h post-procedure, tremor abated completely in the treated hand in 81 essential tremor patients. Imbalance, sensory disturbances and dysarthria were the most frequent acute adverse events. Patients with any adverse event had significantly larger lesions, while inferolateral lesion margins were associated with a higher incidence of motor-related adverse events. Twenty-three lesions were identified with irregular tails, often extending into the internal capsule; 22 of these patients experienced at least one adverse event.

Treatment parameters and lesion characteristics changed with increasing surgeon experience. In later cases, treatments used higher maximum power (normalized to skull density ratio), accelerated more quickly to high power, and delivered energy over fewer sonifications.

Larger lesions were correlated with a rapid rise in both power delivery and temperature, while increased oedema was associated with rapid rise in temperature and the maximum power delivered. Total energy and total power did not significantly affect lesion size. A support vector regression was trained to predict lesion size and confirmed the most valuable predictors of increased lesion size as higher maximum power, rapid rise to high-power delivery, and rapid rise to high tissue temperatures. These findings may relate to a decrease in the energy efficiency of the treatment, potentially due to changes in acoustic properties of skull and tissue at higher powers and temperatures.

We report the largest single surgeon series of focused ultrasound thalamotomy to date, demonstrating tremor relief and adverse events consistent with reported literature. Lesion location and volume impacted adverse events, and an irregular lesion tail was strongly associated with adverse events. High-power delivery early in the treatment course, rapid temperature rise, and maximum power were dominant predictors of lesion volume, while total power, total energy, maximum energy and maximum temperature did not improve prediction of lesion volume. These findings have critical implications for treatment planning in future patients.

1 Department of Neurosurgery, Brigham and Women's Hospital, Harvard Medical School, Boston, MA, USA

2 Department of Neuroscience, Brown University, Providence, RI, USA

3 Department of Neurosurgery, University of California, Los Angeles, CA, USA

4 Department of Radiology, Brigham and Women's Hospital, Harvard Medical School, Boston, MA, USA

Correspondence to: David J. Segar MD

Department of Neurosurgery, Harvard Medical School, Brigham and Women's Hospital, Boston Children's Hospital, Hale Building, 60 Fenwood Road, Boston, MA 02115, USA
E-mail: dsegar@bwh.harvard.edu

Keywords: MR-guided focused ultrasound; thalamotomy; essential tremor

Abbreviations: MRgFUS = MRI-guided focused ultrasound; SDR = skull density ratio

Introduction

The management of medically refractory essential tremor has evolved over the past several decades, as new technologies provided surgeons with a wider array of treatment modalities for ablation or modulation of the ventral intermediate nucleus of the thalamus. Driven by advancements in phased array technology and magnetic resonance (MR) thermometry,^{1–7} ultrasonic thermal lesioning could be done without a craniotomy, and an old neurosurgical lesioning method^{8–11} was taken out of the operating room and into the MRI scanner.¹² Approved in the European Union in 2013 and the FDA in 2016, unilateral MRI guided focused ultrasound (MRgFUS) thalamotomy has emerged as a unique and effective lesioning technique for the treatment of essential tremor^{13,14} and tremor-dominant Parkinson's disease.¹⁵ Ultrasonic lesioning using the existing clinical system is particularly well suited for central targets^{1,16,17} such as the ventral intermediate nucleus of the thalamus, and the procedure is performed awake, with serial clinical testing to track the clinical and behavioural metrics in sync with MR thermographic information regarding the location and heating of the lesioned brain tissue. Furthermore, reversible, low-energy sonifications allow for confirmation of targeting prior to the generation of permanent tissue damage.^{4,18}

As larger numbers of MRgFUS thalamotomies have been performed, those familiar with the technique have begun to further analyse the variables contributing to optimal and sustained tremor reduction, as well as those corresponding to treatment-related side effects.^{19–25} Over the course of multiple clinical trials, tremor outcomes have improved, suggesting that as institutions gained experience with the procedure, small changes in treatment parameters have a tangible positive impact on outcomes.²⁶ Variability still exists in tremor outcomes and the prevalence of adverse events remains higher than reported with deep brain stimulation, though quality of life improvement is dramatic in both cases.^{27–29} While prior studies have demonstrated statistically significant relationships between tremor outcomes and skull density ratio (SDR), patient age, disease duration, peak temperature, a lower number of sonifications, and lesion overlap with specific white matter tracts, these predictors are inconsistent across studies.^{26,27,30–32} The variability seen in prior analyses may be due to pooling of results from different surgeons, relatively low numbers of included patients, and the substantial variability in important factors such as energy delivery strategies, targeting and lesion size.

Currently, methods to predict lesion size based on accumulated thermal dose are impressive,³³ yet our ability to predict lesion size from intra-procedural imaging remains less effective than findings on structural MRI from the day after the procedure was completed.³⁴ Therefore, further improvements in the prediction of lesion size may offer another avenue for improving patient outcomes after MRgFUS.

Here, we report and evaluate 123 cases of MRgFUS thalamotomy for medication-refractory essential tremor and tremor-

dominant Parkinson's disease, performed by a single surgeon at a single institution over 4 years. We report our outcomes and analyse differences in patient-specific variables and energy delivery strategies to demonstrate how these factors may influence the creation of an optimal thalamotomy lesion.

Materials and methods

Patient population

All patients who underwent MRgFUS thalamotomy between March 2016 and June 2020 at the Brigham and Women's Hospital were screened for inclusion in this study, which was approved by the Institutional Review Board. Each patient had a diagnosis of either medication refractory essential tremor or tremor-dominant Parkinson's disease. Of the total 125 patients (Table 1), two were excluded from analysis because of incomplete data: in one case, the patient did not return for an initial postoperative visit. In the second case, treatment was aborted because of failure to elevate temperature above threshold due to cavitation detection. One additional patient did not have axial T₂ sequences obtained on post-procedural Day 1, and was excluded from lesional analysis. Seven patients who were previously enrolled in a multicentre phase III clinical trial were included. A minimum SDR of 0.35 was used as the lower limit for consideration of treatment.

Follow-up and outcomes assessment

Tremor severity was assessed using the Fahn-Tolosa-Marin (FTM) tremor scoring system of the affected limb; tremor was graded on a 5-point scale from 0 to 4, where 0 represents no tremor, and 1–4 represent a graded severity of tremor, from slight to severe.³⁵ Complete Clinical Rating Scale for Tremor (CRST) scores were not obtained outside the patients included in the initial clinical trial. All patients were assessed for baseline tremor preoperatively and on the day after the procedure. At subsequent time points (1 month, 3 months and 1 year), patients were seen in person or via a phone visit when unable to return to the clinic for additional follow-up. Follow-up varied widely depending on patient location and ability to return to the clinic. Adverse effects were categorized in a manner similar to existing literature.³⁰ Events were subsequently graded on level of severity, from grade I (mild) to grade V (mortality), using previously described Clavien-Dindo criteria for the classification of surgical complications.³⁶ Adverse effects reported on post-procedure Day 1 were defined as acute, while those reported at 3-month follow-up were considered persistent, as described in a prior study of focused ultrasound thalamotomy.³⁰ Changes in tremor severity were calculated as a percentage change from preoperative tremor ratings. Analysis of tremor-related outcomes was completed only in patients with a diagnosis of essential tremor ($n = 118$).

Table 1 Demographics and clinical data of included patients (n = 123)

Age, years	75.0 ± 7.42 (55–93)
Percentage males, % (n)	66.6 (82)
Essential tremor, % (n)	96.0 (118)
Tremor-dominant Parkinson's, % (n)	4.1 (5)
Family history of tremor, % (n)	66.6% (82)
Mean duration from diagnosis, years	28.8 ± 18.0 (2–70)
Laterality of thalamotomy, % (n)	
Left	80.5% (99)
Right	19.5% (24)
FTM intention tremor at follow-up (ET only)	
Preop baseline (n = 118)	3.37 ± 0.62 (2–4)
Day 1 (n = 118)	0.33* ± 0.50 (0–2)
3 months (n = 88)	0.47* ± 0.95 (0–4)
1-year follow-up (n = 98)	0.67*** ± 0.96 (0–4)
Treatment parameters	
SDR	0.48 ± 0.08
Number of sonication	10.8 ± 3.60
Maximum power, W	1014 ± 170
Maximum temperature, °C	59.6 ± 5.16
Lesion volume, mm ³	288.98 ± 137.72

Data are presented as % (n) or mean ± SD (range).

*Significant difference from preoperative baseline ($P < 0.0001$).

**Significant difference from Day 1 tremor ($P < 0.01$).

Procedure and treatment parameters

The overall procedural workflow was performed as previously reported at our institution.³⁷ Briefly, all patients underwent pre-operative CT imaging to assess the ratio between cortical and cancellous bone, or SDR. This imaging was also used by the MRgFUS device to correct for skull-induced aberrations.^{1,2} The patient's head was shaved and a modified Cosman-Roberts-Wells frame (Radionics, Inc.) was placed low on the head to accommodate the waterproof silicone seal associated with the ExAblate system. Baseline tremor testing was completed, and the patient was positioned on a 3 T MRI table (GE Medical Systems), before being connected to the ExAblate 4000 MRgFUS hemispheric transducer, operating at 650 Hz (InSightec, Inc.). Cool, degassed water was circulated through the contained space between the head and the transducer to assist in signal transduction and cooling. After obtaining baseline imaging, the ventral intermediate nucleus was localized using a combination of standardized stereotactic coordinates and anatomical landmarks, as the region is not visualizable on standard clinical MRI sequences. Initial target coordinates were one-quarter of the anterior commissure–posterior commissure (AC-PC) distance anterior to the PC, 14 mm from the midline or 11 mm lateral to the wall of the third ventricle and 1.5–2 mm above the AC-PC plane. Three to six subthreshold, low-energy sonication were performed, with temperature and lesion location monitored on MR thermometry to confirm alignment. After confirmation of the finalized target, sonication were delivered sequentially with the goal of reaching a maximum temperature of 55–60 °C in each sonication accompanied by immediate improvement in tremor severity. Clinical testing was performed between each sonication to monitor for both treatment effect and side-effects. With increasing experience, small and progressive changes were made to sonication and targeting strategies.

Imaging and lesion analysis

All patients underwent preoperative CT, which was used by the MRgFUS device to correct for skull-induced aberrations.

Postoperative 3 T MRI was also completed for lesion analysis on the day after the procedure, including thin section axial and coronal T₂ sequences used for analysis. Lesion volumes and surrounding oedema were calculated using the outline of Wintermark zone 2 and zone 3, respectively, on axial and coronal T₂ imaging (Supplementary Fig. 1).³⁸ Wintermark zones 1 and 2 are believed to correlate with coagulation necrosis and cytotoxic oedema, and correlate with the permanent lesion. Zone 3 is thought to represent transient vasogenic oedema, often seen on 24-h and 1-week imaging.³⁸ Approximate lesion centre was determined using axial T₂ images at the level of the AC-PC plane, and ellipsoid lesion volumes were calculated using the maximal distances along axial, coronal and sagittal axes. Relationships between the lesion and the wall of the third ventricle and internal capsule were measured in the AC-PC plane. The superior and inferior extent of the lesion was measured in relation to the intercommissural plane. Irregularities in lesion shape were not detectable using this methodology, and represent a limitation of our analysis; however, visual inspection of all lesions was performed to identify consistently irregular features and their relationship with surrounding structures.

Statistical analysis

Univariate analyses were performed using two-sided t-tests. In this study, a false negative is of high consequence, as we are looking to identify any possible contributors to tremor reduction, adverse effects, lesion size and shape; therefore, adjustment for multiple comparisons was not performed for univariate analyses. Two sample proportion tests were used to compare proportions between two groups. Spearman's rank correlation coefficients (ρ) were used to evaluate continuous (monotonic) relationships between treatment parameters. Averages are reported as means ± standard deviation. High-power and high-energy sonication were defined as those in the top 33% after aggregating across all sonication from all patients. Statistical analysis was performed in Python 3.8, using tools derived from standard scientific computing packages.^{39,40}

SDR normalized values of power and energy were calculated using a linear regression between the SDR and mean power or mean energy, respectively, and fitted to a linear equation. For each patient, SDR values were used to calculate the expected mean power based on the regression equation. Power or energy values for that patient were divided by their expected mean, such that a value > 1 corresponded to a value above the expected mean.

Multivariate linear support vector regression (SVR) models were created to evaluate predictors of thalamotomy lesion volume. Continuous and discrete numerical input values of the SVR were imputed with means, and missing output values were not considered. For all models, scikit-learn 0.23.1 in Python 3.8 was used. The linear SVR models were trained with a hinge loss and a regularization parameter of 1.0.

A null distribution was created for each model, in which the input training data were shuffled prior to training. The empirical testing data were then tested for accuracy. Accuracy values were represented as a fraction, and for continuous values, a Pearson regression was calculated. Models were run on 100 Monte-Carlo randomly shuffled cross-validations, with one-third of the data held out for testing and two-thirds used for training. To assess the overall distributions from the empirical and shuffled model performance, the distributions of performance values were also compared by calculating an area under the curve (AUC) value for the receiver operator characteristic. A single empirical AUC value was calculated to denote the separability of the shuffle distribution and the empirical distribution. The empirical AUC value was then

compared to a null distribution comprised of 1000 AUC values from shuffling the two distributions. Feature coefficients from the linear SVR were also assessed. The significance of each feature coefficient was assessed with a similar AUC bootstrap and corrected for multiple comparisons with a Bonferroni correction with $\alpha = 0.05$.

Features from a 'full model' were removed in a stepwise fashion, guided by the AUC significance and overall model performance. Features from this initial model are available in [Supplementary Table 4](#).

Data availability

The data that support the findings of this study are available from the corresponding author, upon reasonable request.

Results

Patient demographics and tremor outcomes are noted in [Table 1](#). Mean patient age was 75.0 ± 7.42 years (range: 55–93); 33% ($n = 41$) were female. Mean disease duration was 28.8 ± 18.0 (range: 2–70) years. Significant bilateral tremor was most prevalent, with 55% of patients ($n = 68$) experiencing greater tremor on the right and 21% ($n = 26$) with greater tremor on the left. Eighteen per cent ($n = 22$) had right-sided tremor only, and 6% ($n = 7$) had only left-sided tremor. Consistent with the disease process, baseline tremor in the 118 patients with essential tremor (as measured by the Fahn-Tolosa-Marin rating scale of the affected limb, from 0 to 4) was predominantly mild in the head, voice and affected extremity at rest, with significant postural (2.68 ± 0.82) and intention (3.37 ± 0.62) tremor. Eighty per cent of all patients ($n = 99$) underwent left-sided thalamotomy.

In essential tremor patients, intention tremor in the treated limb was reduced acutely by 90.2%, and by 86.2% at 3 months. In patients with 1-year follow-up ($n = 98$), intention tremor reduction averaged 80.0% below baseline. Postural and rest tremor completely abated after thalamotomy, and remained well controlled at 3-month and 1-year follow-up. As intention tremor has proven more relevant to patient disability and is more difficult to control after surgical intervention,⁴¹ subsequent tremor analyses are limited to intention tremor.

Tremor reduction

Immediately following treatment, tremor in the treated upper extremity abated completely in 81 of 118 patients with essential tremor. Postoperative intention tremor scores in the treated hand were significantly decreased from preoperative baselines ([Fig. 1](#)) at all time points, with a slow upward trend in mean tremor score over the first year ([Table 1](#)).

Percentage tremor reduction on Day 1 was weakly correlated with increasing institutional experience ($\rho = 0.19$, $P = 0.037$), while no other individual parameter demonstrated a significant correlation with acute tremor reduction. While the first and last 25 patients had similar preoperative intention tremor scores (3.29 versus 3.52, $P = 0.144$), acute tremor reduction in the affected limb of the first and last 25 patients was 84.03% and 94.2%, respectively ($P = 0.013$), potentially demonstrative of a learning curve.

Lesion size and location correlate with adverse effects

Adverse effects were analysed in both essential tremor and Parkinson's disease patients after MRgFUS. Intraoperatively, several treatment-related side effects were noted by the surgeon,

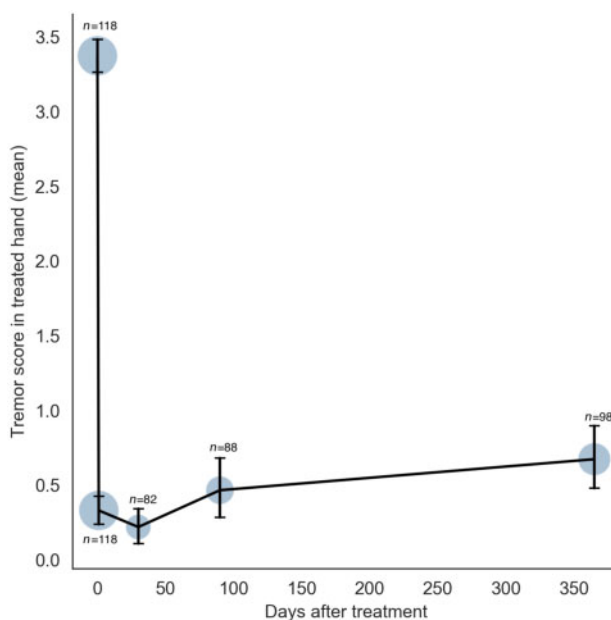


Figure 1 Average intention tremor scores over time. One hundred and eighteen patients with essential tremor were included. Mean preoperative intention tremor scores are reported and compared with available intention tremor scores at 24 h, 1 month, 3 months, and 1-year follow-up. Circles correspond to the size of the cohort at follow-up. Error bars represent standard deviations.

though frequency of occurrence was not recorded; headache was common, as was a sensation of movement during the sonifications, sometimes described as the sensation of falling backwards. Transient face or hand numbness was less commonly reported intraoperatively. In one case, a patient experienced nausea and vomiting requiring a transient cessation of treatment.

Adverse effects on post-procedure Day 1 were defined as acute, while those ongoing at 3-month follow-up were considered persistent.³⁰ All adverse effects were categorized as mild (grade I) by Clavien-Dindo criteria. Gait imbalance was, by far, the most common acute adverse effect noted ($n = 74$), followed by sensory disturbances, dysarthria, dysmetria, motor weakness, and dysgeusia ([Table 2](#)). Certain adverse effects, particularly motor-related effects, co-occurred frequently. ([Supplementary Table 1](#)). In a majority of cases (54.4%), patients with any acute adverse effects were likely to also experience imbalance.

Lesion location and size were associated with the occurrence of these adverse effects. Lesions in patients with imbalance, dysmetria, sensory and motor symptoms, and dysgeusia were larger than those without those adverse effects. When grouped together, patients with any acute adverse effect had larger lesions (300.5 mm^3 versus 229.21 mm^3 , $P = 0.0184$), more oedema ($P = 0.047$), more inferior ($P = 0.0062$) and lateral ($P = 0.0027$) lesion margins than those without ([Fig. 2D](#)). These differences in volume were significant for imbalance, sensory and speech related adverse effects and approached significance for dysmetria. Differences in lesion margins were significant for gait imbalance, but often trended towards significance for other adverse effects.

In the 74 patients with gait imbalance, lesions were larger (306.8 mm^3 versus 250.3 mm^3 , $P = 0.0037$). Lesion margins average 0.65 mm further inferior ($P = 0.0017$), 0.98 mm closer to the internal capsule ($P = 0.002$), and 0.63 mm more anterior ($P = 0.032$) than those without imbalance ([Fig. 2A](#)).

Acute sensory adverse effects occurred in 32 patients ([Supplementary Fig. 2](#)). The lesions in these patients were larger

(352.9 mm^3 versus 260.1 mm^3 , $P = 0.001$). Posterior lesion margin was also 0.37 mm closer to the PC, though this difference was not significant ($P = 0.094$).

Twenty-six patients experienced acute dysarthria. In these patients, lesions were significantly larger (353.2 mm^3 versus 265.8 mm^3 , $P = 0.005$) than in patients without dysarthria (Fig. 2B). Lesion margins were 0.53 mm more inferior ($P = 0.127$) and 0.74 mm closer to the internal capsule ($P = 0.085$). Dysarthria was slightly more common in patients with left-sided thalamotomies (22.2%, 22/99) as compared to those with right-sided thalamotomies (16.7%, 4/24), but these differences were not significant ($P = 0.550$).

Patients with acute dysmetria ($n = 15$) also commonly experienced gait imbalance (12/15, 80%). Similar to imbalance, lesions associated with acute dysmetria were larger (356.6 mm^3 versus 274.4 mm^3 , $P = 0.057$) and extended, on average, 0.62 mm further below the intercommissural plane than those without ($P = 0.10$) (Fig. 2C).

Lesions associated with acute motor weakness ($n = 11$) had margins 0.94 mm closer to the internal capsule in the AC-PC plane ($P = 0.11$). In contrast, the distance from lesion centre to third ventricular wall was only 0.1 mm larger in patients experiencing weakness, highlighting the importance of patient-specific anatomy when targeting. Upon visual inspection of these 11 lesions, 9 (81.8%) had irregular T_2 hyperintense tails extending obliquely away from the ellipsoid lesion volume and into the internal capsule (Fig. 3).

Twenty-two of 23 patients (95.7%) with a capsular tail experienced at least one adverse event, suggesting that this currently unpredictable radiographic finding may have a high positive predictive value for the presence of adverse events, particularly motor-related effects.

No patients reported acute dysgeusia, but six patients noted dysgeusia in a delayed fashion at different time points. No statistically significant features were noted in these patients.

Adverse effects improved over time (Table 2). Of 123 total patients, 90 were evaluated at 3-month follow-up, and 100 were evaluated at 1 year, with decreasing rates of gait imbalance, dysmetria, sensory symptoms, motor weakness and dysarthria at

each time point, though loss to follow-up prevents definitive conclusions about changes in adverse events over time.

Sonication parameters differentially affect lesion volume and oedema volume

Consistent with prior reports,^{23,42–44} patients with higher SDR required lower power and energy over the course of the procedure, and maximum temperature was positively correlated with SDR (Supplementary Fig. 2).

With increasing surgeon and institution experience, small but deliberate changes were made to sonication-related parameters, affecting both lesion volume and oedema (Fig. 4A–F). While maximum temperature decreased slightly in later cases ($\rho = -0.2$, $P = 0.034$), high temperatures ($> 56^\circ\text{C}$) were reached earlier in the procedure ($\rho = -0.41$, $P < 0.0001$; Fig. 4C), accompanied by a faster rate of energy delivery, as high-power sonications were delivered earlier in the treatment course ($\rho = -0.58$, $P < 0.0001$) over fewer total sonications ($\rho = -0.68$, $P < 0.0001$). The slower rates of energy delivery early in our experience reflect, in part, an abundance of caution with a new technology, but these changes in treatment parameters offer an opportunity to evaluate the effects of treatment parameters on lesion generation.

As sonication parameters changed with institutional experience, so too did lesion characteristics. Lesion volume increased with experience ($\rho = 0.31$, $P = 0.0006$; Fig. 4E), increasing most rapidly over the first 40 cases, then levelling out at an average of 322.9 mm^3 over the remaining cases, closely mirroring the changes in early, high power delivery (Fig. 4C). Despite these larger lesions, overall rates of adverse effects in the first and last 25 patients were not significantly different on Day 1 (15 versus 21, $P = 0.059$), or at 3 months (12 versus 13, $P = 0.777$), or 1-year follow-up (five versus two, $P = 0.221$).

Perilesional oedema initially trended up alongside lesion volume, but then began to downtrend back to levels comparable to earlier in the series (Fig. 4F). This relative decrease in perilesional oedema volume to lesion volume in the later portion of the series highlights that changes in energy delivery strategies may differentially affect lesion volume and oedema volume. Observation of

Table 2 Adverse events

Adverse events (ET and PD)	1 Day postoperative (n = 123)	1 Month postoperative (n = 87)	3 Months postoperative (n = 90)	1 Year postoperative (n = 100)
Motor weakness	11 (9%)	13 (15%)	6 (7%)	3 (3%)
Face	4 (4)	1 (1)	–	–
Limb	3 (3%)	11 (13%)	6 (7%)	3 (3%)
Face and limb	4 (2%)	1 (1%)	–	–
Dysarthria	26 (21%)	11 (13%)	7 (8%)	6 (6%)
Sensory deficits (paraesthesia/numbness)	32 (26%)	26 (33%)	22 (25%)	17 (17%)
Orofacial	22 (18%)	20 (30%)	14 (16%)	11 (11%)
Orofacial and finger	8 (7%)	5 (6%)	5 (6%)	6 (6%)
Fingers	2 (2%)	1 (2%)	3 (3%)	–
Gait imbalance	74 (60%)	40 (46%)	23 (26%)	15 (15%)
Dysgeusia	0 (0%)	5 (6%)	6 (7%)	3 (3%)
Dysmetria	16 (13%)	15 (17%)	8 (9%)	7 (7%)
Headache	5 (4%)	3 (3%)	–	–
Hypotension/ lightheadedness	2 (2%)	1 (1%)	–	–

Data are presented as n (%). ET = essential tremor; PD = Parkinson's disease

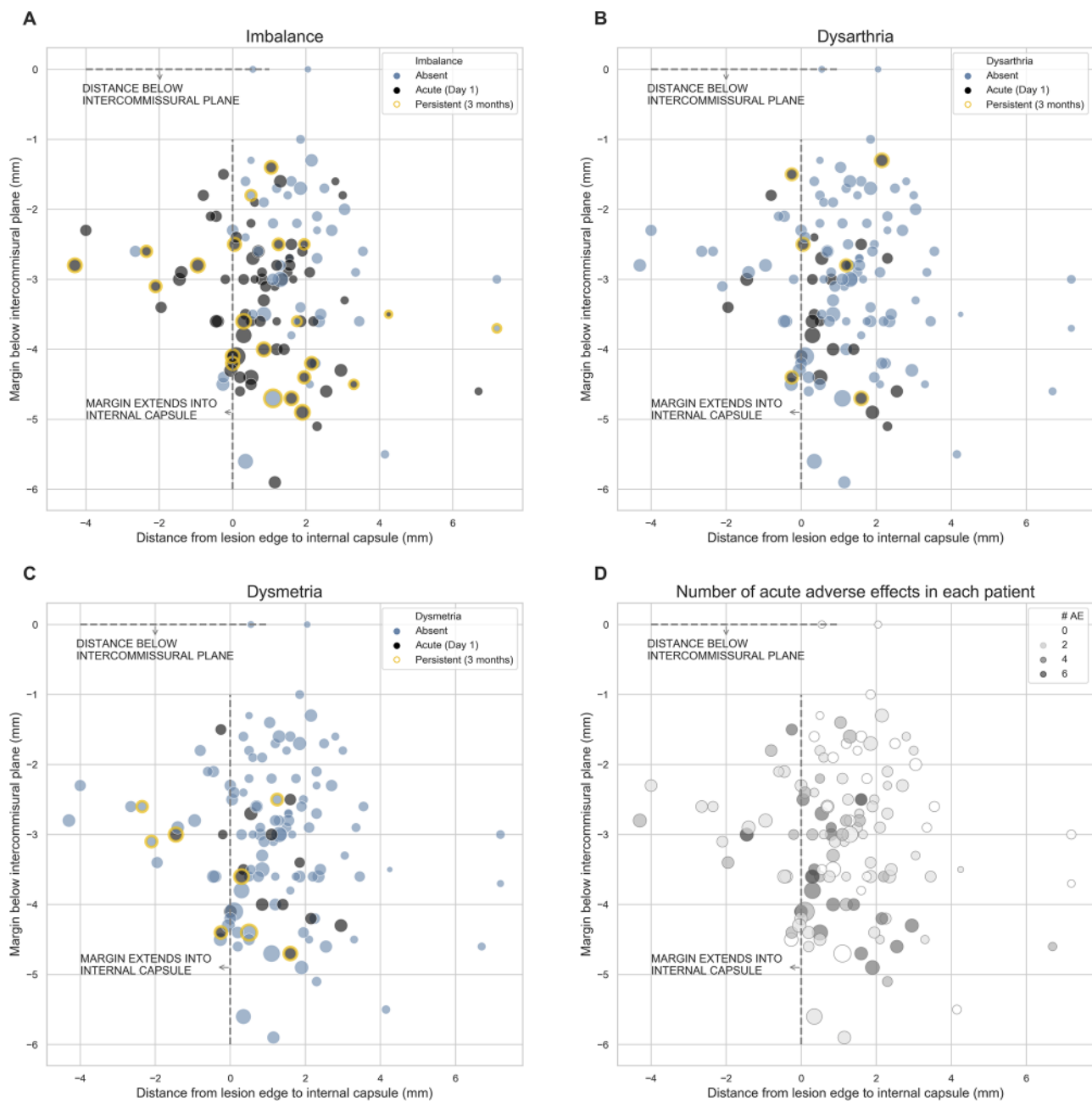


Figure 2 Lesion volume, inferior and lateral margins are high risk for adverse effects. Larger lesion volumes, lateral and inferior lesion margins are associated with acute adverse effects. (A–C) The distribution of lesion volumes, inferior margins (distance below intercommissural plane) and lateral margins (distance from lateral margin to the internal capsule) are noted in patients with acute and persistent imbalance (A), dysarthria (B), and dysmetria (C). (D) Inferior and lateral lesions also corresponded with a larger number of adverse events in each patient.

these changes provided additional clues about the relationships between treatment parameters and lesion characteristics.

The rapid acceleration of energy delivery and temperature correlates with larger lesions

Lesion size was correlated with SDR ($\rho = 0.27$, $P = 0.0036$), and surprisingly, was negatively correlated with total number of sonications ($\rho = -0.23$, $P = 0.011$). The maximum Euclidean distance travelled between the original sonication target and subsequent adjusted targets was, unsurprisingly, also correlated with larger lesion volume ($\rho = 0.2$, $P = 0.037$). However, mean, maximum and total power did not correlate with lesion volume,

and neither did mean, maximum or total energy. Because the expected sonication power required for a given patient is inversely correlated with SDR, the linear relationship between SDR and mean power was quantified with linear regression ($R = 0.33$, $P < 0.0001$), and raw power values were normalized by SDR to account for expected differences in patient-specific power delivery (Fig. 5A). After normalizing for SDR, maximum power ($\rho = 0.20$, $P = 0.049$) and mean power ($\rho = 0.21$, $P = 0.038$) trended towards significant correlation with lesion size.

To understand the relationship between sonication parameters and lesion volume, individual sonication curves were evaluated. To quantify the effects of magnitude and timing of power delivery on lesion size, we aggregated power across all sonications and all

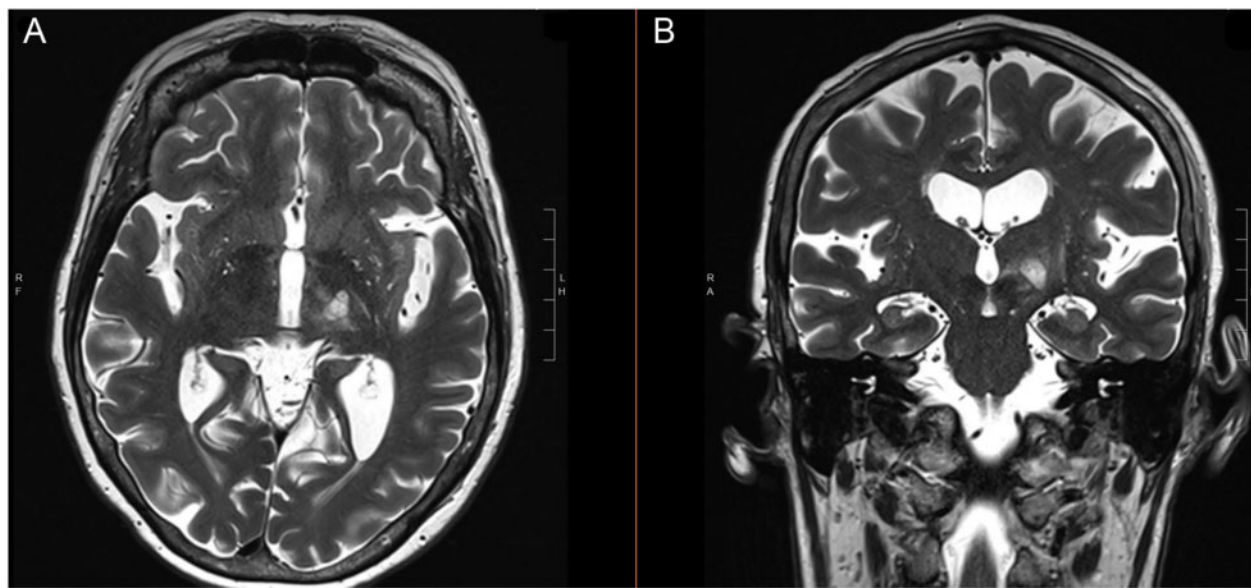


Figure 3 Capsular lesion tails. Irregular lesional tails, seen in the axial (A) and coronal (B) planes on T₂ MRI, were in some cases noted to extend into the internal capsule. These lesional tails correlated strongly with motor weakness.

patients, and defined 'high-power sonifications' as those in the top 10%. The total number of high-power sonifications in a given treatment did not correlate with increased lesion size ($\rho = 0.073$, $P = 0.47$). However, when high-power sonifications were delivered earlier in the treatment course, lesions were in fact larger ($\rho = 0.29$, $P = 0.0029$; Fig. 5A).

Similarly, the impact of temperature varied with timing. Maximum temperature achieved in a given lesion weakly correlated with lesion size ($\rho = 0.2$, 0.033). But when temperatures $>56^\circ\text{C}$ were achieved earlier in the treatment course, lesions were significantly larger ($\rho = -0.35$, $P = 0.0003$; Fig. 5B). This temperature threshold is a common goal for maximal temperature in focused ultrasound thalamotomy, and also corresponds with results from Bond and Elias,³⁴ who suggest that to achieve a thermal lesion of at least 5 mm on post-procedure Day T₂ imaging, peak voxel temperatures would likely need to exceed 56°C . Earlier heating to $>56^\circ\text{C}$ ($\rho = -0.2$, $P = 0.037$) and higher normalized maximum power ($\rho = 0.2$, $P = 0.040$) both correlated with increased oedema.

Multivariate modelling confirms rapid rise in power and temperature as important predictors of lesion volume

A multivariate SVR was trained to evaluate the most impactful predictors of lesion volume from available treatment parameters. Fourteen treatment-related variables considered to have a potential impact on lesion volume were included (Supplementary Table 4).

This initial model was reduced to a refined model with improved predictive value. In this final model (Fig. 6), the model performed with an R² of 0.45 ($P < 0.0001$) using five input variables. Variables in the initial model that either worsened or did not change the predictive power of the model were removed in a stepwise fashion. The variables contributing to the final model of lesion volume included: the sonication number at which temperature rose above 56°C , the maximum distance between sonication targets, early delivery of high-power sonifications, SDR and maximum power (SDR-normalized). Notably, total power, energy and duration, number of sonifications, maximum energy and

maximum temperature did not strengthen prediction of lesion volume.

Discussion

Our reported clinical outcomes reaffirm findings described in prior studies of tremor reduction after MRgFUS.^{14,26,45} The tremor improvement observed in our study is similar to earlier studies that have reported an average acute tremor improvement in the affected extremity from 35% to 90% with a pooled average of 62%.²⁷ Consistently, tremor relief is greatest in the immediate postoperative period with some waning of effect during follow-up period, but with durable long-term efficacy.^{24,27,30,32,45} However, tremor improvement remains durable with long-term follow-up.^{24,32,45} The incidence of adverse events reported in our series is also in line with reported literature.^{27,30} In our results and in prior studies, imbalance and sensory deficits have been observed to be the most common side effects following treatment, and inferolateral lesions appear to present the most substantial risk for motor-related side effects.³⁰ Consistent with our outcomes, nearly all adverse events reported in earlier studies have been reported as mild, and improve over time.²⁷ It is important to note that mild but persistent adverse effects such as gait imbalance may still prove consequential for patient outcome, potentially increasing the risk of falls over time.

The impact of lesion volume on outcomes is complex, and different targeting strategies may be prudent when planning larger or smaller lesions. While some have argued that larger thalamotomy lesions are more effective at suppressing tremor,^{46,47} citing 40 mm³ as the minimum volume required to produce benefit, others have not found such a relationship,³⁰ and in our series, tremor reduction was not significantly correlated with lesion volume. One reason for this may be that our lesions averaged 289 mm³ and ranged from 25 mm³ to 895 mm³, larger than lesions in many other series. On average, a larger volume may be more likely to overlap with areas of optimal tremor suppression, which likely resides at the border of the ventral intermediate and ventral caudal nuclei.^{30,31,48} Conversely, our results and others have demonstrated a significant relationship between lesion volume and rates of adverse

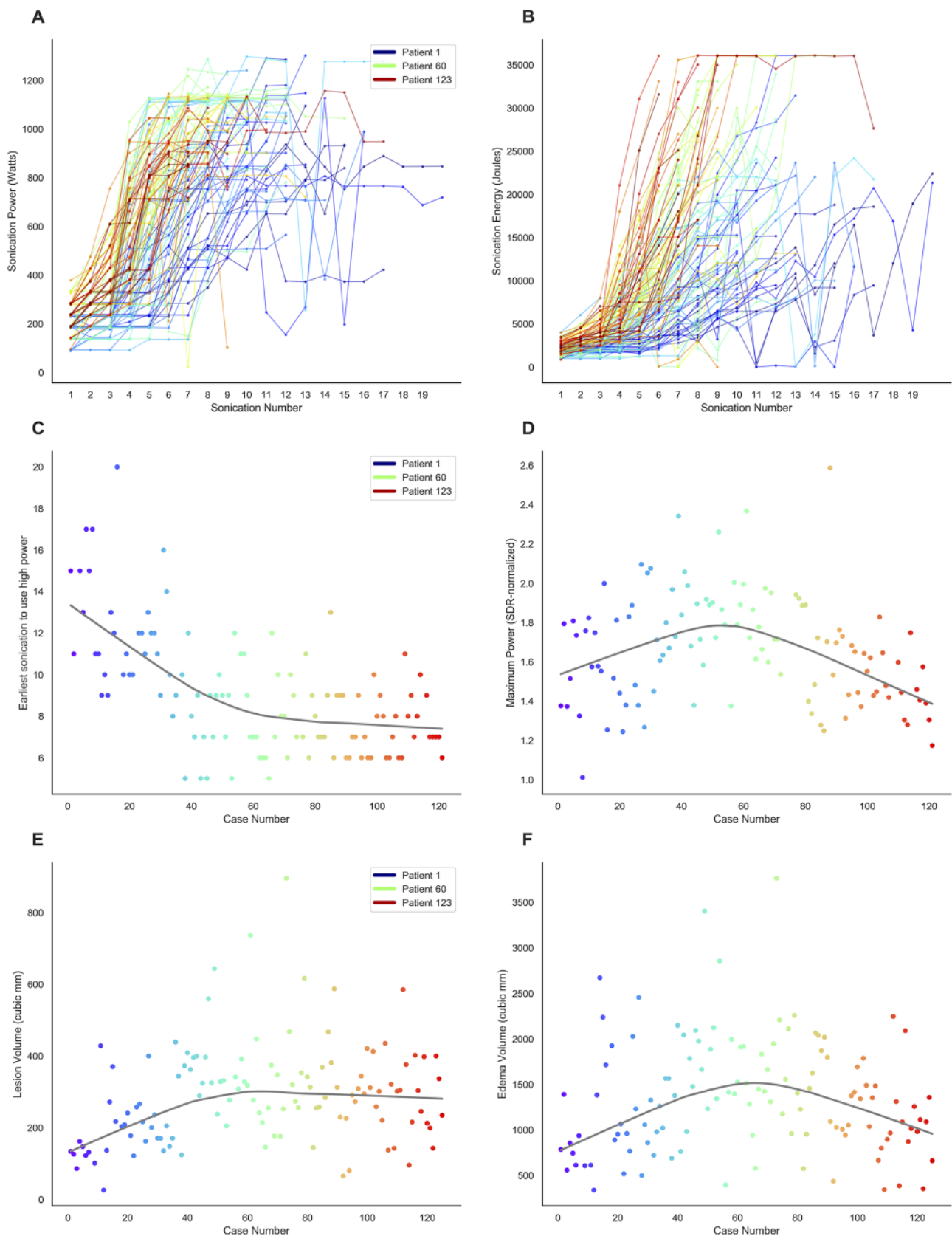


Figure 4 Sonication parameters and lesion volumes changed with increasing experience. Changes in energy delivery, lesion volume and oedema changed with increasing experience. In each panel, values from individual patients are represented by the same colour, with early patients represented by dark blue, and the most recent patients represented in red. Sonication values of power (A) and energy (B) over the course of treatment are represented by each line, with increasing experience, power and energy were delivered more rapidly over fewer sonications. Later cases reached high power (top 10% of sonication powers) during earlier sonications (C), while maximum power delivery (normalized to expected power based on SDR) increased, but subsequently decreased with increasing experience (D). Increases in lesion volume (E) mirrored the earlier delivery of high power, while increases in oedema (F) more closely mirrored normalized maximum power delivery.

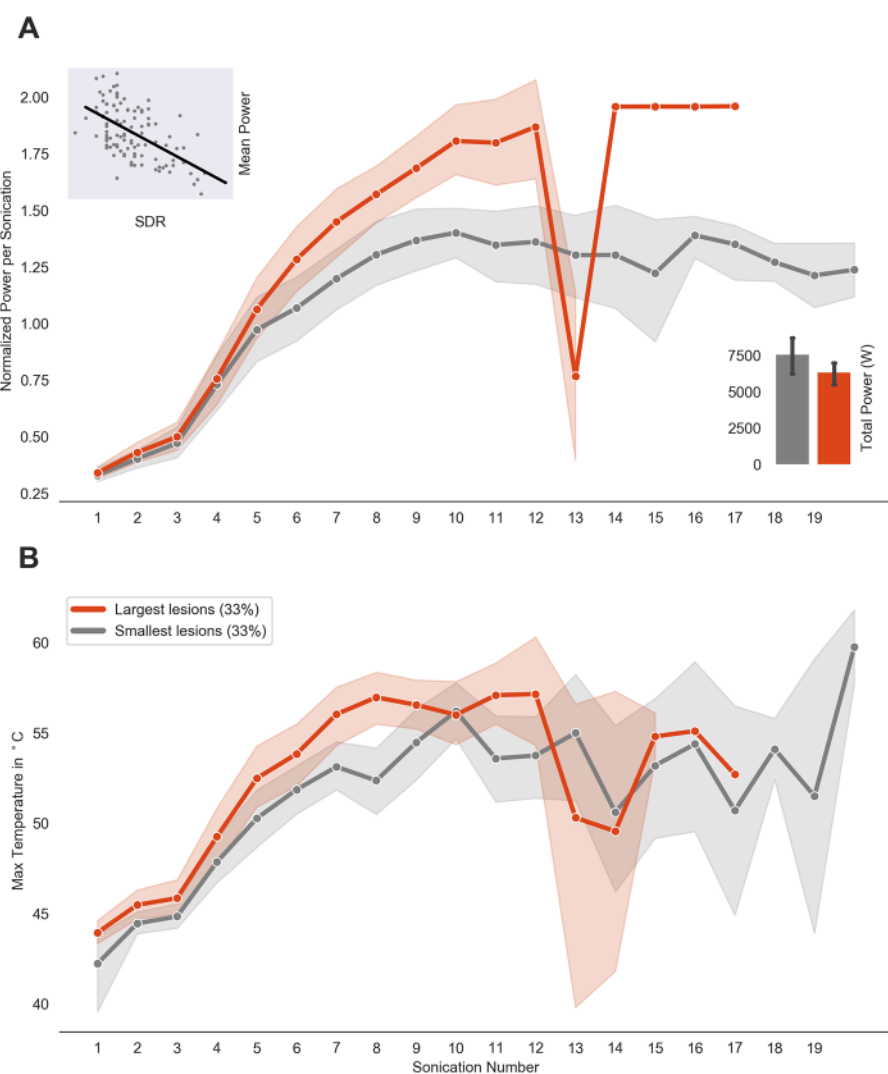


Figure 5 Power and temperature per sonication. Timing of power delivery and temperature rise relate to lesion volume. To control for differences in expected power delivery based on SDR, power values were normalized based on the expected mean power determined by linear regression (A, top left inset). On average, the largest 33% of lesions delivered power earlier, reached higher maximum normalized power (A), but delivered less total power over the procedure (A, bottom right inset). (B) The largest lesions also reached high temperatures earlier in the procedure.

events. In Boutet et al.,³⁰ lesions above 170 mm³ were associated with increased rates of adverse events. Our lesions were generally larger than this threshold, but our targeting strategies likely differed from the Toronto group, Boutet et al.,³⁰ as our lesions were intentionally centred more medially and superiorly to provide a buffer for larger lesion volumes, away from inferolateral zones defined as high risk for adverse events.³⁰ The differences highlighted by these two series reinforce the importance of the interplay between lesion location and lesion volume. It is also worth noting that targeting for MRgFUS must rely on different coordinates used for radiofrequency or deep brain stimulation—at our institution, we now plan targets approximately 2 mm above rather than at the level of the AC-PC plane to account for inferior expansion of the lesion.

Our clinical-anatomical relationships were also consistent with those described by Boutet et al.³⁰ More posterior lesions were more likely to result in sensory side effects as they approach the ventral caudal nucleus of the thalamus. Lesions encroaching on the internal capsule were more likely to cause motor-related side effects, such as gait imbalance, weakness and dysarthria, and those extending inferiorly towards dentato-thalamic pathways

were more likely to cause dysmetria, dysarthria and gait imbalance. While no specific anatomic biases were associated with the infrequent occurrence of dysgeusia in our series, others have described a similar association between thalamic lesioning or infarction and taste disturbances,^{49–51} likely implicated by the gustatory relays from the solitary tract, via the posteromedial ventral nucleus of the thalamus to the contralateral cortex.⁵²

To maintain a durable treatment effect and reduce adverse effects, the ideal lesion should be accurately placed and large enough to allow for durable tremor reduction, but as small as possible, to minimize encroachment on nuclei or tracts associated with adverse effects. This goal is aided by identifying high-risk areas such as the inferior and lateral regions seen in our data (Fig. 2) and in Boutet et al.³⁰ Combining these findings with tractography³¹ or direct visualization of the thalamic nuclei^{48,53} may prove particularly valuable for determining optimal patient-specific targets. Methods we developed to use the thermometry phase imaging during treatment to visualize the internal capsule and other anatomy may also be helpful to refine atlas-based targeting.⁵⁴

Even if an ideal lesion location, size and shape can be planned preoperatively, technical and patient-specific considerations such

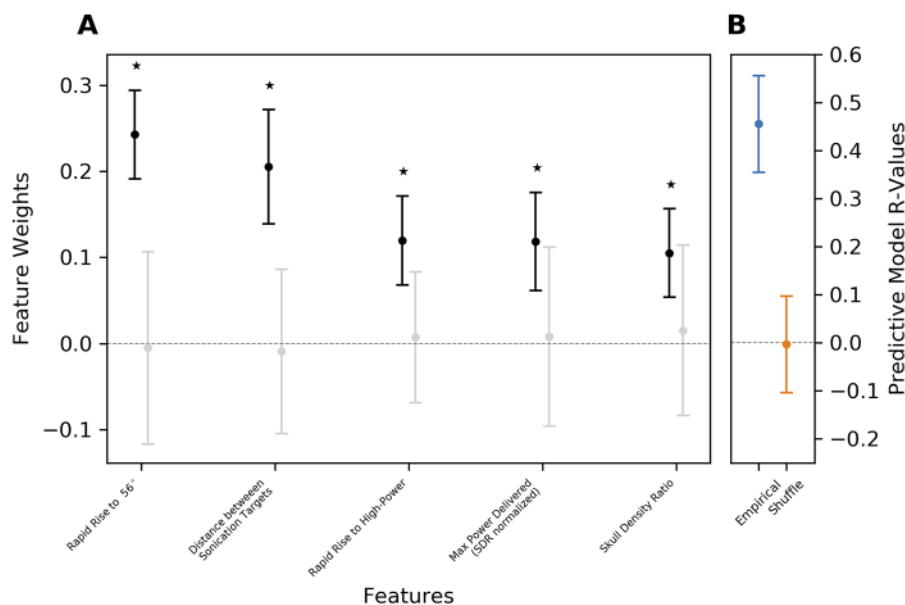


Figure 6 Predictive model of lesion volume. (A) Results from a support vector regression demonstrate the features most predictive of lesion volume, in order of decreasing feature weight, with error bars representing standard deviations. Each feature in this final model performed significantly greater than chance ($P < 0.0001$). (B) Overall, the model performed with an $R = 0.45$.

as treatment efficiency may complicate the creation of an optimal lesion and increase the risk of unexpected adverse effects. One such example is the decrease in energy efficiency identified on MR thermometry at high power resulting in dispersion of heating at the target, which leads to heating of a larger tissue volume.⁵⁵ Our data demonstrate that high maximum power delivery and rapid delivery of high energy is in fact associated with larger lesions on post-procedural MRI. In addition, incremental increases in tissue temperatures also decrease heating efficiency.^{34,56} This finding may explain why early high-energy sonications and early temperature rise predicted larger lesions in our data. Because early high-power delivery and rapid heating lead to larger lesions over a smaller number of treatment sonications, it is worth noting that there may be less room for error when delivering energy rapidly.

We have noted other technical challenges that may limit our ability to create lesions of adequate volume. In certain instances, the occurrence of cavitation limits our ability to use desired high powers, therefore requiring more extended, lower energy treatments, which may limit possible lesion size. Patients with low SDR may also require energies near the maximum allowed by the system, and lesion size per sonication will be small. Both patient discomfort and the long cooling times required between sonications may limit the lesion size that can be obtained; while not recorded in our series, these data would be of value in future investigations of lesion size.

As we better understand additional contributors to lesion volume, these factors might be used to synchronize more perfectly our lesion planning and monitoring with our ultimate lesion creation. To that end, we utilized a predictive machine learning regression to quantify several factors predictive of lesion volume, which might help a treatment team better estimate lesion size based on treatment parameters prior to energy delivery. Our prediction achieved an R^2 of 0.45 without the contribution of thermal dose estimates obtained from MR thermometry, which correlate strongly with lesion size. Recent contributions have shown robust relationships between lesion size on post-procedural MRI and thermal dose models, achieving correlation coefficients of 0.44–0.89^{34,57,58} and Sorenson-Dice coefficients of 0.69–0.81.^{33,59} However, preoperative prediction could potentially be improved by

identifying additional patient-specific and treatment-related features associated with changes in lesion size, such as those we have described here, and which we hypothesize are related to changes in treatment efficiency.^{55,56} Combining available data from accumulated thermal dose and the additional power, temperature and heating efficiency metrics presented here could move us closer to creating predictive models of lesion size that are highly reliable and can better augment procedural planning and decision making.

In our patients, we identified an uncommon but consequential asymmetric lesional tail, which in several cases caused weakness via extension into the internal capsule and was overwhelmingly associated with adverse events. While these tails were often identified on MR thermometry as they occurred, subsequent adjustments to targeting or energy delivery did not always prevent undesired effects. The skewed lesion shape is, in part, a consequence of the distortion of spherical waves by the oblate geometry of the skull and may be partially corrected by temporal edge filters on the MRgFUS machine. However, predicting significant irregularities in lesion shape remains challenging, and is of significant clinical importance given the strong association with motor weakness and adverse events more generally.

Despite a large patient population, our follow-up after post-procedure Day 1 varies substantially. While this presents a challenge when reporting outcomes, many of our patients have travelled a distance to undergo this procedure and follow-up was tailored to individual patient needs. Furthermore, we only recorded tremor scores in the affected limb, and did not collect complete CRST scores. We recognize that this limits conclusions that might be drawn about long-term efficacy and adverse events. In clinical environments such as ours, we hope to see further development of tools enabling clinical follow-up without requiring an in-person visit. Some such tools do exist,⁶⁰ but would require further validation before they could be considered as replacement for validated rating scales.

MRgFUS is a relatively new therapy, and while effective for tremor reduction, optimal treatment strategies are still being explored. High-volume centres may still have significant differences in their methods, as optimal targeting, lesion size and energy

delivery strategies are considered. While rates of tremor reduction may be somewhat less durable than can be achieved with deep brain stimulation,²⁸ the primary drawback of MRgFUS remains higher rates of adverse events. Nevertheless, the minimally invasive nature allows for treatment of patients who might otherwise be poor candidates for awake surgery or general anaesthesia, and increasing procedural experience, patient-specific targeting, and improvements in lesion prediction may also help improve the adverse event profile. While we have excellent tools to monitor and predict our lesion creation, continuing to improve our ability to translate our desired plan into a reproducible and predictable lesion should improve the safety and reliability of this new treatment modality.

Acknowledgements

We would like to thank Sarah Christie, PA-C for her excellent care of the patients in this study. In addition, we deeply appreciate the dedication of the BWH Radiology nurses and technologists who make these procedures possible.

Funding

No funding was received towards this work.

Competing interests

G.R.C. has received clinical research support from InSightec Inc.

Supplementary material

[Supplementary material](#) is available at Brain online.

References

- Clement GT, White J, Hynynen K. Investigation of a large-area phased array for focused ultrasound surgery through the skull. *Phys Med Biol.* 2000;45(4):1071–1083.
- Aubry JF, Tanter M, Pernot M, Thomas JL, Fink M. Experimental demonstration of noninvasive transskull adaptive focusing based on prior computed tomography scans. *J Acoust Soc Am.* 2003;113(1):112.
- Pernot M, Aubry JF, Tanter M, Thomas JL, Fink M. High power transcranial beam steering for ultrasonic brain therapy. *Phys Med Biol.* 2003;48(16):2577–2589.
- Hynynen K, McDannold N. MRI guided and monitored focused ultrasound thermal ablation methods: A review of progress. *Int J Hyperthermia.* 2004;20(7):725–737.
- Hynynen K, Clement GT, McDannold N, et al. 500-element ultrasound phased array system for noninvasive focal surgery of the brain: A preliminary rabbit study with ex vivo human skulls. *Magn Reson Med.* 2004;52(1):100–107.
- Hynynen K, McDannold N, Clement G, et al. Pre-clinical testing of a phased array ultrasound system for MRI-guided noninvasive surgery of the brain—A primate study. *Eur J Radiol.* 2006; 59(2):149–156.
- Marquet F, Pernot M, Aubry J-F, et al. Non-invasive transcranial ultrasound therapy based on a 3D CT scan: Protocol validation and in vitro results. *Phys Med Biol.* 2009;54(9):2597–2613.
- Lynn JG, Zwemer RL, Chick AJ. The biological application of focused ultrasonic waves. *Science.* 1942;96(2483):119–120.
- Lynn JG, Zwemer RL, Chick AJ, Miller AE. A new method for the generation and use of focused ultrasound in experimental biology. *J Gen Physiol.* 1942;26(2):179–193. doi:10.1085/jgp.26.2.179
- Fry WJ, Barnard JW, Fry EJ, Krumins RF, Brennan JF. Ultrasonic lesions in the mammalian central nervous system. *Science.* 1955;122(3168):517–518.
- Harary M, Segar DJ, Huang KT, Tafel IJ, Valdes PA, Cosgrove GR. Focused ultrasound in neurosurgery: A historical perspective. *Neurosurg Focus.* 2018;44(2):E2.
- Hynynen K, Jolesz FA. Demonstration of potential noninvasive ultrasound brain therapy through an intact skull. *Ultrasound Med Biol.* 1998;24(2):275–283.
- Lipsman N, Schwartz ML, Huang Y, et al. MR-guided focused ultrasound thalamotomy for essential tremor: A proof-of-concept study. *Lancet Neurol.* 2013;12(5):462–468.
- Elias WJ, Lipsman N, Ondo WG, et al. A randomized trial of focused ultrasound thalamotomy for essential tremor. *N Engl J Med.* 2016;375(8):730–739.
- Bond AE, Shah BB, Huss DS, et al. Safety and efficacy of focused ultrasound thalamotomy for patients with medication-refractory, tremor-dominant Parkinson disease: A randomized clinical trial. *JAMA Neurol.* 2017;74(12):1412–1418.
- Hughes A, Hynynen K. Design of patient-specific focused ultrasound arrays for non-invasive brain therapy with increased trans-skull transmission and steering range. *Phys Med Biol.* 2017;62(17):L9–L19.
- Jung NY, Rachmilevitch I, Sibiger O, Amar T, Zadicario E, Chang JW. Factors related to successful energy transmission of focused ultrasound through a skull: A study in human cadavers and its comparison with clinical experiences. *J Korean Neurosurg Soc.* 2019;62(6):712–722.
- Hynynen K, Vykhotseva NI, Chung AH, Sorrentino V, Colucci V, Jolesz FA. Thermal effects of focused ultrasound on the brain: Determination with MR imaging. *Radiology.* 1997;204(1):247–253.
- Chang WS, Jung HH, Kweon EJ, Zadicario E, Rachmilevitch I, Chang JW. Unilateral magnetic resonance guided focused ultrasound thalamotomy for essential tremor: Practices and clinical-coradiological outcomes. *J Neurol Neurosurg Psychiatry.* 2015; 86(3):257–264.
- Zaaroor M, Sinai A, Goldsher D, Eran A, Nassar M, Schlesinger I. Magnetic resonance-guided focused ultrasound thalamotomy for tremor: A report of 30 Parkinson's disease and essential tremor cases. *J Neurosurg.* 2018;128(1):202–210.
- Fishman PS, Elias WJ, Ghanouni P, et al. Neurological adverse event profile of magnetic resonance imaging-guided focused ultrasound thalamotomy for essential tremor. *Mov Disord.* 2018; 33(5):843–847.
- Meng Y, Solomon B, Boutet A, et al. Magnetic resonance-guided focused ultrasound thalamotomy for treatment of essential tremor: A 2-year outcome study. *Mov Disord.* 2018;33(10): 1647–1650.
- D'Souza M, Chen KS, Rosenberg J, et al. Impact of skull density ratio on efficacy and safety of magnetic resonance-guided focused ultrasound treatment of essential tremor. *J Neurosurg.* 2020;132(5):1392–1397.
- Park Y-S, Jung NY, Na YC, Chang JW. Four-year follow-up results of magnetic resonance-guided focused ultrasound thalamotomy for essential tremor. *Mov Disord.* 2019;34(5):727–734.
- Fukutome K, Kuga Y, Ohnishi H, Hirabayashi H, Nakase H. What factors impact the clinical outcome of magnetic resonance imaging-guided focused ultrasound thalamotomy for essential tremor? *J Neurosurg.* 2021;134(5):1618–1623.
- Krishna V, Sammartino F, Cosgrove R, et al. Predictors of outcomes after focused ultrasound thalamotomy. *Neurosurgery.* 2020;87(2):229–237.
- Mohammed N, Patra D, Nanda A. A meta-analysis of outcomes and complications of magnetic resonance-guided focused

- ultrasound in the treatment of essential tremor. *Neurosurg Focus*. 2018;44(2):E4.
28. Harary M, Segar DJ, Hayes MT, Cosgrove GR. Unilateral thalamic deep brain stimulation versus focused ultrasound thalamotomy for essential tremor. *World Neurosurg*. 2019;126:E144–E152.
 29. Giordano M, Caccavella VM, Zaed I, et al. Comparison between deep brain stimulation and magnetic resonance-guided focused ultrasound in the treatment of essential tremor: A systematic review and pooled analysis of functional outcomes. *J Neurol Neurosurg Psychiatry*. 2020;91(12):1270–1278.
 30. Boutet A, Ranjan M, Zhong J, et al. Focused ultrasound thalamotomy location determines clinical benefits in patients with essential tremor. *Brain*. 2018;141(12):3405–3414.
 31. Tsolaki E, Downes A, Speier W, Elias WJ, Pouratian N. The potential value of probabilistic tractography-based for MR-guided focused ultrasound thalamotomy for essential tremor. *NeuroImage Clin*. 2018;17:1019–1027.
 32. Sinai A, Nassar M, Eran A, et al. Magnetic resonance-guided focused ultrasound thalamotomy for essential tremor: A 5-year single-center experience. *J Neurosurg*. 2020;133(2):417–424.
 33. McDannold NJ, White PJ, Cosgrove GR. MRI-based thermal dosimetry based on single-slice imaging during focused ultrasound thalamotomy. *Phys Med Biol*. 2020;65(23):235018.
 34. Bond AE, Elias WJ. Predicting lesion size during focused ultrasound thalamotomy: A review of 63 lesions over 3 clinical trials. *Neurosurg Focus*. 2018;44(2):E5.
 35. Fahn S, Tolosa E, Concepcion M. Clinical rating scale for tremor. In: J Jankovic, J Tolosa, eds. *Parkinson's Disease and Movement Disorders*. Williams and Wilkins; 1993: 271–280.
 36. Dindo D, Demartines N, Clavien P-A. Classification of surgical complications. *Ann Surg* 2004;240(2):205–213.
 37. Harary M, Essayed WI, Valdes PA, McDannold N, Cosgrove GR. Volumetric analysis of magnetic resonance-guided focused ultrasound thalamotomy lesions. *Neurosurg Focus*. 2018;44(2):E6.
 38. Wintermark M, Druzgal J, Huss DS, et al. Imaging findings in MR imaging-guided focused ultrasound treatment for patients with essential tremor. *AJR Am J Neuroradiol*. 2014;35(5):891–896.
 39. Harris CR, Millman KJ, van der Walt SJ, et al. Array programming with NumPy. *Nature*. 2020;585(7825):357–362.
 40. Virtanen P, Gommers R, Oliphant TE, et al. SciPy 1.0 Contributors. SciPy 1.0: Fundamental algorithms for scientific computing in Python. *Nat Methods*. 2020;17(3):261–272.
 41. Tsuboi T, Jabarkheel Z, Zeilman PR, et al. Longitudinal follow-up with VIM thalamic deep brain stimulation for dystonic or essential tremor. *Neurology*. 2020;94(10):e1073–e1084.
 42. Chang WS, Jung HH, Zadicario E, et al. Factors associated with successful magnetic resonance-guided focused ultrasound treatment: Efficiency of acoustic energy delivery through the skull. *J Neurosurg*. 2016;124(2):411–416.
 43. Boutet A, Gwun D, Gramer R, et al. The relevance of skull density ratio in selecting candidates for transcranial MR-guided focused ultrasound. *J Neurosurg*. 2020;132(6):1785–1791.
 44. McDannold N, White PJ, Cosgrove R. Elementwise approach for simulating transcranial MRI-guided focused ultrasound thermal ablation. *Phys Rev Res*. 2019;1(3):033205.
 45. Halpern CH, Santini V, Lipsman N, et al. Three-year follow-up of prospective trial of focused ultrasound thalamotomy for essential tremor. *Neurology*. 2019;93(24):e2284–e2293.
 46. Hirai T, Miyazaki M, Nakajima H, Shibasaki T, Ohye C. The correlation between tremor characteristics and the predicted volume of effective lesions in stereotactic nucleus ventralis intermedius thalamotomy. *Brain J Neurol*. 1983;106 (4):1001–1018.
 47. Nagaseki Y, Shibasaki T, Hirai T, et al. Long-term follow-up results of selective VIM-thalamotomy. *J Neurosurg*. 1986;65(3): 296–302.
 48. Su JH, Choi EY, Tourdias T, et al. Improved Vim targeting for focused ultrasound ablation treatment of essential tremor: A probabilistic and patient-specific approach. *Hum Brain Mapp*. 2020;41(17):4769–4788.
 49. Fujikane M, Itoh M, Nakazawa M, Yamaguchi Y, Hirata K, Tsudo N. [Cerebral infarction accompanied by dysgeusia—a clinical study on the gustatory pathway in the CNS. *Rinsho Shinkeigaku*. 1999;39(7):771–774] [in Japanese].
 50. Gilard V, Maltête D, Lefaucheur R, Chastan N, Derrey S. Dysgeusia following ventral intermediate nucleus deep brain stimulation for essential tremor. *Parkinsonism Relat Disord*. 2014; 20(11):1307–1308.
 51. Carlson JD, McLeod KE, Mark JB, McLeod PS, Bremer BA. Dysgeusia in deep brain stimulation for essential tremor. *J Clin Neurosci*. 2018;50:242–246.
 52. Heckmann JG, Heckmann SM, Lang CJG, Hummel T. Neurological aspects of taste disorders. *Arch Neurol*. 2003;60(5):667–671.
 53. Tourdias T, Saranathan M, Levesque IR, Su J, Rutt BK. Visualization of intra-thalamic nuclei with optimized white-matter-nulled MPRAGE at 7T. *NeuroImage*. 2014;84:534–545.
 54. McDannold N, White PJ, Cosgrove GR. Using phase data from MR temperature imaging to visualize anatomy during MRI-guided focused ultrasound neurosurgery. *IEEE Trans Med Imaging*. 2020;39(12):3821–3830.
 55. Hughes A, Huang Y, Schwartz ML, Hyynnen K. The reduction in treatment efficiency at high acoustic powers during MR-guided transcranial focused ultrasound thalamotomy for essential tremor. *Med Phys*. 2018;45(7):2925–2936.
 56. Yamamoto K, Ito H, Fukutake S, et al. Factors associated with heating efficiency in transcranial focused ultrasound therapy. *Neurol Med Chir (Tokyo)*. 2020;60(12):594–599.
 57. Huang Y, Lipsman N, Schwartz ML, et al. Predicting lesion size by accumulated thermal dose in MR-guided focused ultrasound for essential tremor. *Med Phys*. 2018;45(10):4704–4710.
 58. Jones RM, Kamps S, Huang Y, et al. Accumulated thermal dose in MRI-guided focused ultrasound for essential tremor: Repeated sonication with low focal temperatures. *J Neurosurg*. 2019;132(6):1802–1809.
 59. Seasons GM, Mazerolle EL, Sankar T, et al. Predicting high-intensity focused ultrasound thalamotomy lesions using 2D magnetic resonance thermometry and 3D Gaussian modeling. *Med Phys*. 2019;46(12):5722–5732.
 60. Sanderson JB, Yu JH, Liu DD, et al. Multi-dimensional, short-timescale quantification of Parkinson's disease and essential tremor motor dysfunction. *Front Neurol*. 2020;11: 886.